ISSN: 0974-5823 Vol. 7 No. 8 August, 2022

International Journal of Mechanical Engineering

The Impact of Lateral Stiffness on the Structural Performance of Hybrid Open Web Steel Joists Using Rebar Waists

Haitham H. Muteb

Civil Engineering Department, University of Babylon, Babylon, Iraq

Jenan N. Almusawi

Civil Engineering Department, University of Kufa, Babylon, Iraq

How to Cite: **Haitham H. Muteb, Jenan N. Almusawi (2021). The Impact of Lateral Stiffness on the Structural Performance of Hybrid Open Web Steel Joists Using Rebar Waists. International Journal of Mechanical Engineering 6(1), pp.1-4.**

Abstract Open Web Steel Joists (OWSJs) are truss-type members because they can transmit both tensile and compressive pressures while using less material by using the waists of rebars as a diagonal member, resulting in lower costs and a lower self-weight, as well as reducing vibration noticeability. The purpose of this study is to investigate the influence of lateral stiffness by presenting three prefabricated models (A, B, and C) of a new product of (HOWSJs), where model A represents less stiffness, model B moderate stiffness, and model C stiffness. The results of the experiments showed that the cross-sectional shape of (HOWJs) had a significant effect on the behavior of the steel joist, with the ultimate capacity of the HOWSJ specimens of (Model A) increasing by almost (7.4 percent) and (14.5 percent), respectively, when compared to specimens of (Model B) and (Model C). The ductility index of the (Model C) specimens was 1.52 and 1.35 times that of the (Model A) and (Model B) specimens, respectively.

Index Terms - Experimental Investigation, Steel Joist, Welded Angles, Rebar Waists, Lateral Stiffness, Ductility Index

1. INTRODUCTION

Buckling analysis is especially important because steel structures are slender systems, and it occurs suddenly and causes the system to collapse. The behavior of prefabricated steel joists and joist girders (PFSJGS) proposed in this paper, such as lateral torsional buckling, must be investigated. Steel joists are strong and stiff in plane, but very flexible out of plane. As a result, they must be properly braced before any construction load is applied. They are constructed of a flexible interior shear web that supports the top and bottom chords, and their cross-sections are frequently mono-symmetric or unsymmetrical. Due to the fact that hot-rolled I-beams have relatively continuous thick webs that prevent web local and flange distortional buckling, the lateral torsional buckling behavior of (PFSJGS) is more complex than that of doubly symmetric hot-rolled beams. In addition, the material properties of steel joist sections, such as yield stress, vary significantly depending on where the cross section is located. The residual stress pattern in open web steel joists differs dramatically from that of hot-rolled I-beams. Despite the widespread use of open web steel joists, methods for designing them to resist lateral torsional buckling are inadequate.

Previous research on the lateral-torsional buckling of steel beams has primarily focused on hot-rolled steel beams. Timoshenko and Gere [1] were the first to investigate the critical elastic lateral-torsional buckling of I-

beams analytically. Bradford and Wee [2] put eight hot-rolled steel I-beams to the test, with seats at the ends. The buckling mode is distortional because the top compressive flange is only restrained by the stiffness of the web. Zirakian and Showkati [3] conducted distortion buckling experiments on simply supported fabricated steel I-beams with a central concentrated load and an effective lateral brace at the mid-span of the top compression flange, and the experimental beam strengths were compared to the design strengths predicted by the American AISC/LRFD [4] and the Australian AS4100 [5] specifications. Generally, the two specifications provide un-conservative predictions in the inelastic range of structural response as the beam length decreases and inelastic behaviour becomes more intense. Also, there are many researches about cold formed steel beams.

Winter et al. [6] carried out biaxial bending and torsion tests on cold-form channel beams (CFCs) loaded eccentrically through their webs. lateral buckling tests of simply supported and unbraced cold-formed steel lipped channel beams subjected to mid-span loading were performed by Put et al. [7]. A numerical study by Pi et al. [8] conducted to investigate the elastic lateral–distortional buckling, inelastic behaviour and strengths of cold-formed steel beams and developed improved design rules for lateral distortional buckling. Zhao et al. [9] conducted lateral buckling tests of cold-formed steel RHS beams. An analytical model by Chu et al. [10] was proposed an analytical model for predicting the lateral torsional buckling of thin-walled channel beams that are partially laterally restrained by metal sheeting and subjected to uplift loading. Nirosh and Mahen [11] conducted a numerical study was undertaken to investigate the lateral–torsional buckling behaviour of simply supported cold-formed steel lipped channel beams subjected to uniform bending.

It can be seen that there have been very few reports of experiments conducted on the lateral buckling of OWSJ , thus the purpose of this paper is to conduct experiments and a detailed parametric study based on 3D finite element model using ABAQUS analyses was undertaken to fully understand the lateral torsional buckling behaviour of OWSJ. The $OWSJ_S$ in this paper are prefabricated using steel angles for the top and bottom chords and steel reinforcing bars for inner web elements. Since the result is a light structure, the result is a delicate stability structure in its various modes.

2. LATERAL BUCKLING TEST

1.1 Material properties

According to the ASTM (A 370-15) [12] nine tension tests were carried out on coupons, three tension coupons were cut from the two legs of angle (50*50*4), three from plate (175*50*3.8), and three from reinforcing steel bar with diameter (11.97 mm). The mean tensile yield stress (Fy) and according to the results of the tests for angles was (334.9 MPa) , for reinforcing bars with diameter (11.97 mm) was (554 MPa), and it was (321.89 MPa) for the plate of (3.8mm) thick. The prefabricated steel joist girders have been welded by using the E6013 wire electrode according to AWS A5.1 requirements [13].

1.2 Steel joist girders

Three models of simply supported prefabricated hybrid open web steel joists (PHOWSJs) with different cross section shapes were tested, each model consist of two specimens having the same cross section. The span (L) of all models is constant (1800 mm) to produce the main differences in the lateral torsional buckling in different cross section shapes of steel joist. The (PHOWSJs) were made using steel angles (L50*50*4) mm for the top and bottom chords and steel reinforcing bars with (11.97 mm) diameter for inner web elements with diagonal rebars (Ldb=357 mm) and vertical rebars (Lvb=350 mm). The details of the (PHOWSJs) and the shape of cross section are shown in ‘Figure 1’. The nominal cross section dimensions and properties of these sections are shown in (Table 1) where the moments of inertia of (PHOWSJs) were calculated as a built-up section, (h) the overall depth of the joist.

Table 1.

Nominal cross section dimensions and sections properties of (PHSJGs).

Groups	Specimen No.	Cross Section Shape	Dimensions (mm)		Moment of Inertia (mm^4)	
			b_f	h	I_x	I_y
Model A	SJ 1-1 SJ 1-2	Section (1)	100	350	40892537.76	646597.76
Model B	SJ 2-1 SJ 2-2	Section (2)	100	350	40892537.76	2420437.76
Model C	SJ 3-1 SJ 3-2	Section (3)	200	350	40892537.76	11974277.76

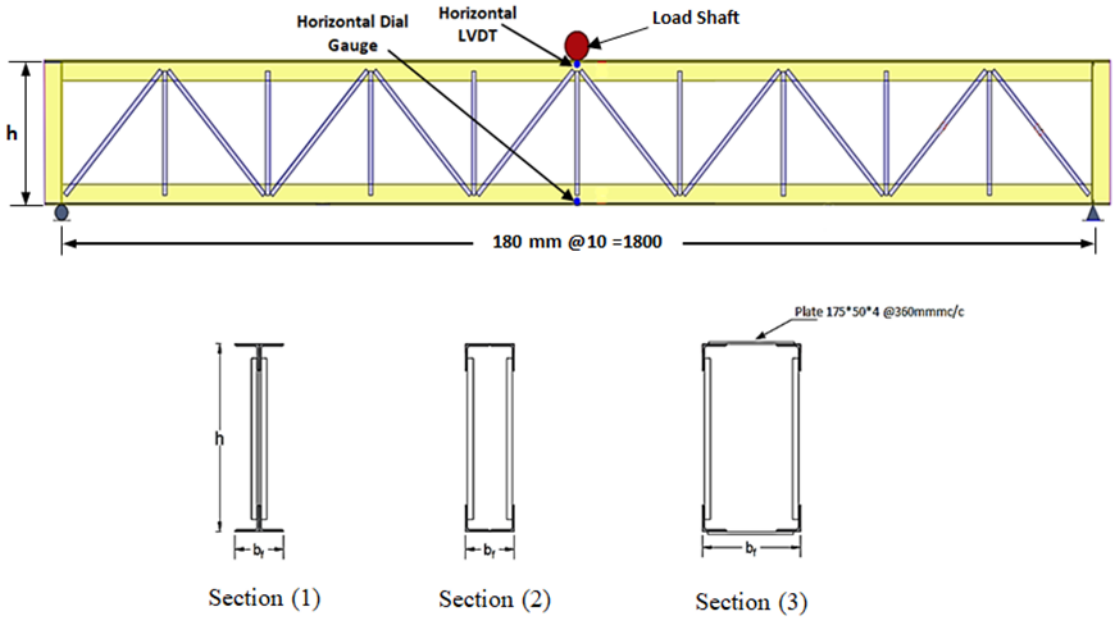

Figure 1.

Steel joist girder (all dimensions in mm).

1.3 Supports

The beam supports restrained for lateral buckling shown in 'Figure 2' were intended to provide simple supports that prevent the lateral deflection and twist rotation as possible in the ends of the steel joist specimen during the test, this shape of support called fork support.

1.4 Loading

Six simply supported (PHSJGs) were be tested under a single concentrate static load on the top flange up to failure by using a steel shaft with diameter (25 mm) as shown in 'Figure 2'.The load was applied using hydraulic testing machine with capacity 1000 kN in Structures Laboratory at Kufa University.

1.5 Experimental Displacement Measurements

At the mid span of the joist the top displacements (u_{uf}) were measured using linear variable displacement transducers (LVDT), and the lower displacements (u_{lf}) were measured using a digital dial gauge and its data

has been recorded using camera, 'Figure 2'. The rotation of the lateral buckling (ø) was calculated 'as in equation (1)'.

$$\phi = \tan^{-1}\frac{u}{h_1} = \tan^{-1}\frac{(u_{uf} - u_{lf})}{h_1} \quad (1)$$

where u_{uf}: the measured lateral displacement of the top flange of HOESJ

u_{lf}: the measured lateral displacement of the bottom flange of HOESJ

h_1 : the distance between u_{uf} and u_{lf} .

By using the above formula, the load- deformation curves (P-u) and (P- ϕ) can be plotted for all models.

3. TEST RESULTS

For each specimen a summary of the lateral buckling test results for the maximum load, maximum lateral deflection, and maximum rotation can be listed in Table (2).

Table (2):

lateral buckling test results for HOWSJ specimens

Models	Specimen No.	Ultimate Load P_u (kN)	Max. Lateral Deflection ($u_{max.}$) (mm)	Max. Rotation (ϕ_{max}) (degrees)
Model A	SJ 1-1	101.34	3.178	0.669
	SJ 1-2	100.65	3.302	0.701
Model B	SJ 2-1	94.24	3.991	0.803
	SJ 2-2	92.81	3.834	0.779
Model C	SJ 3-1	84.97	11.995	2.438
	SJ 3-2	87.65	12.234	2.487

2.1Load – Lateral Deflection Curves

Load versus lateral deflection curves at the mid-span of all the ten specimens were plotted and introduced in Figures (3) to (5) where each one introduces the results of two specimens for the same model.

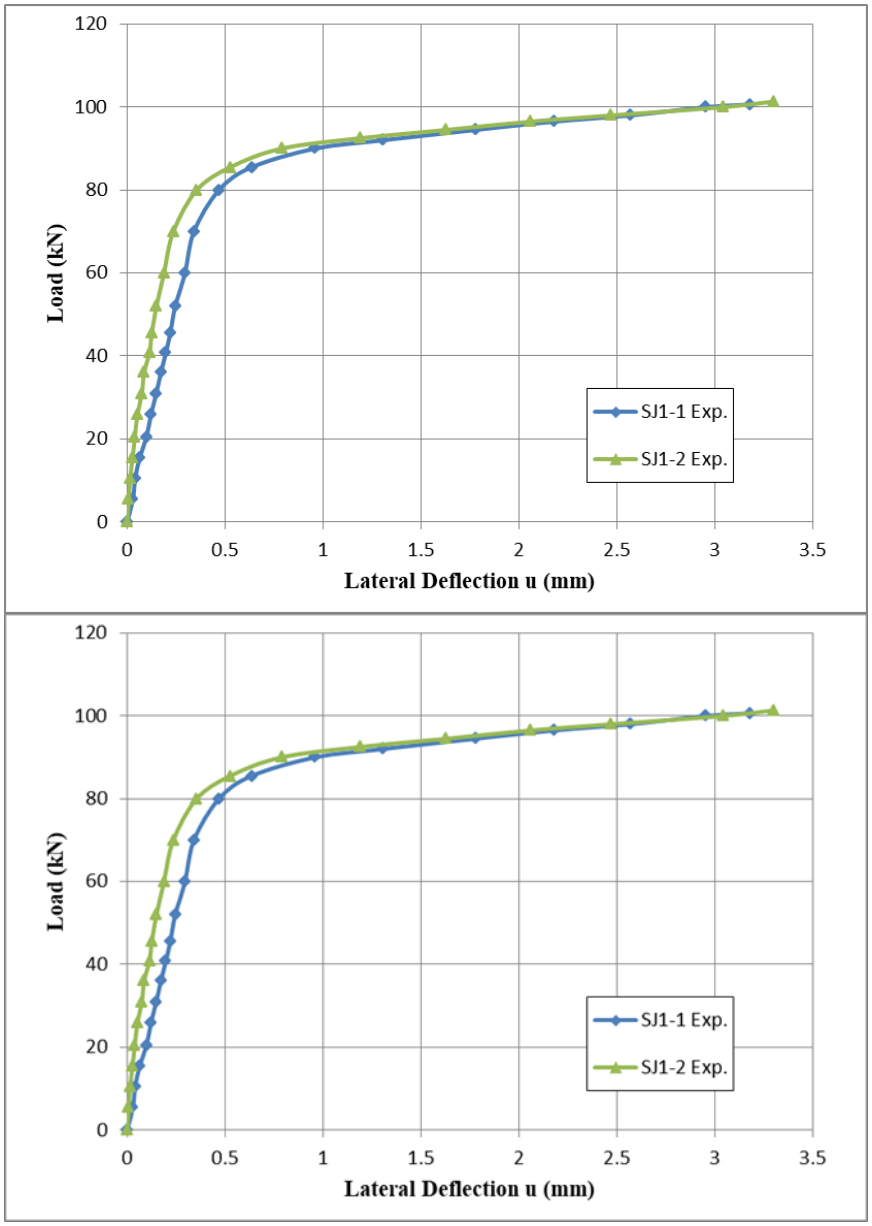

Figure 3.

Load- Lateral Deflection Curve for SJ1-1 and SJ1-2 Specimens.

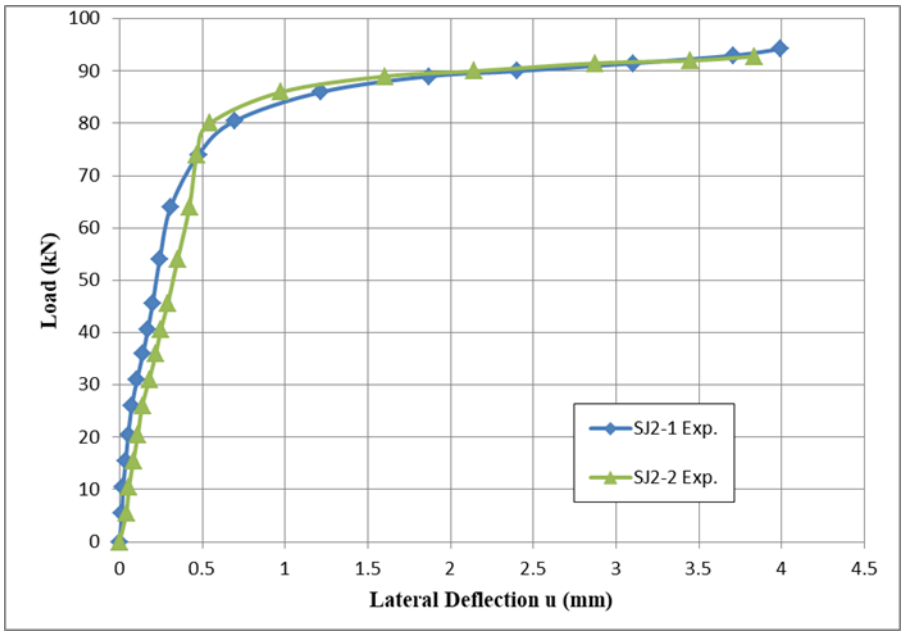

Figure 4.

Load- Lateral Deflection Curve for SJ2-1 and SJ2-2 Specimens.

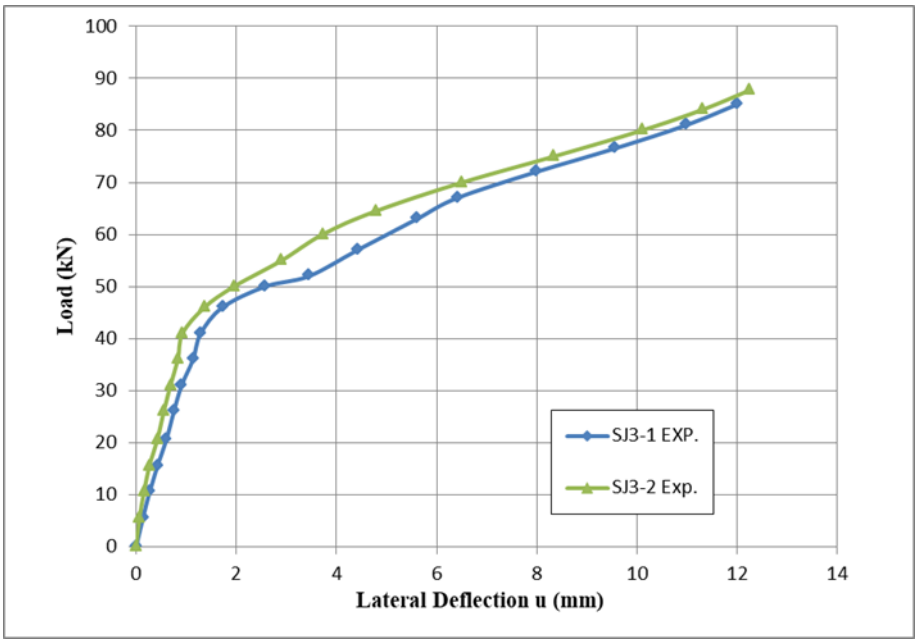

Figure 5.

Load- Lateral Deflection Curve for SJ3-1 and SJ3-2 Specimens.

2.2Load – Rotation Curves

Load versus lateral deflection curves at the mid-span of all the ten specimens were plotted and introduced in Figures (6) to (8) where each one introduces the results of two specimens for the same model.

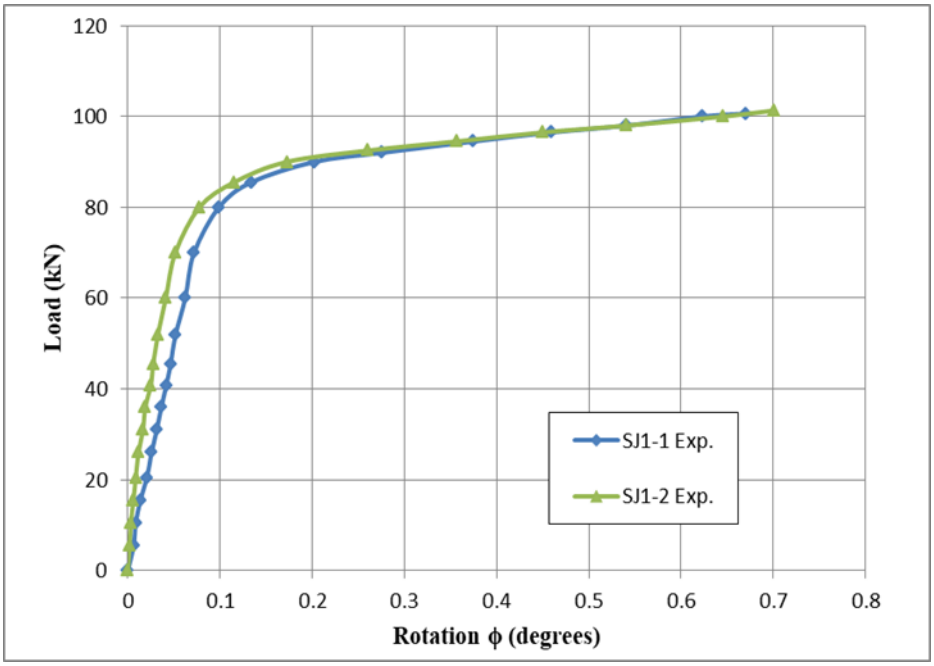

Figure 6.

Load- Rotation Curve for SJ1-1 and SJ1-2 Specimens.

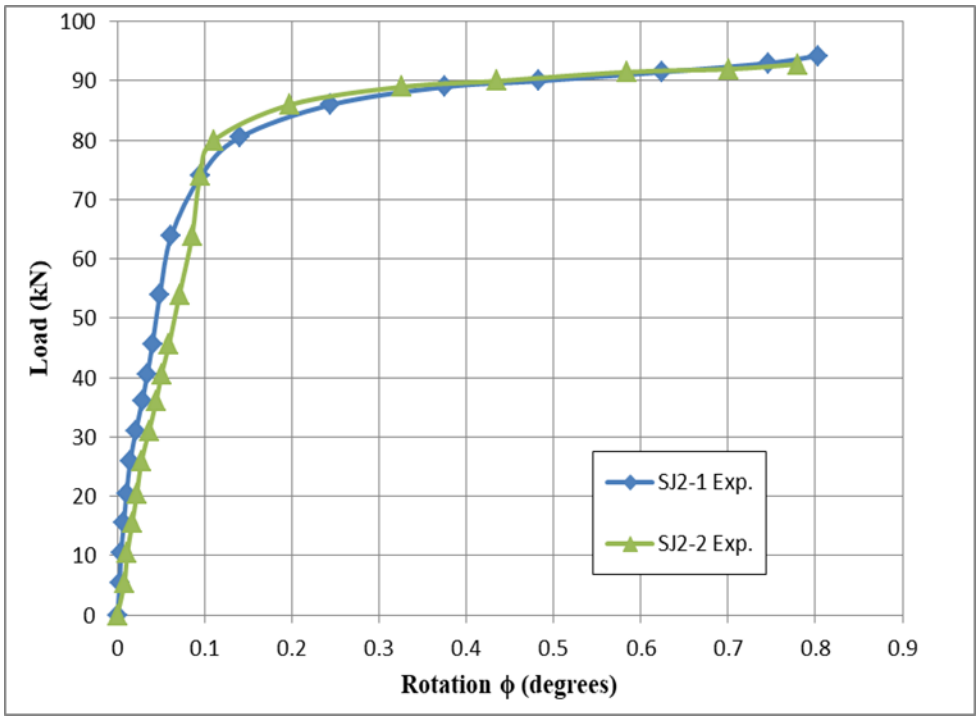

Figure 7.

Load- Rotation Curve for SJ2-1 and SJ2-2 Specimens.

2.3Failure Mechanism

From the previous curves it can observed that every two specimens of each model had the same behavior, thus to compare the results for different models, the average measured out of deformations of each two HOWSJ specimens for the same model was displayed in Table (3) considering the experimental lateral torsional buckling capacity to be defined as the maximal force measurement at which inelastic deformations and collapse occurred, thus (P_u) presented the recorded LTB capacity of HOWS joist used in this work. Also Figures (9) and (10) showed a comparison between the behavior for all models, where the mean value for each two specimens for the same model were plotted.

From these curves it can be noticed that Model A had a small lateral deflections and rotations while the joist was still elastic, but these increased as the load increased towards the elastic lateral buckling load and they accelerated after yielding originated, and reached relatively high values as the failure load was approached. The experimental test displayed that for Model A specimens test specimens the same ultimate failure mechanism was observed, which was a buckling of the compression top flange (horizontal leg of the top chord angles). And a very small local buckling in the mid span diagonal interior web member were occurred, and all HOWSJ specimens for these three models had a slightly lateral buckling during the loading phase until they reached their ultimate capacity. While there was no local buckling observed on the vertical leg of the top chord angles. This mode of failure called flexural lateral torsional buckling, Plate (1) displayed the failure mode of this model.

For Model C specimens, it can be seen from Figures (9) and (10) that the HOWSJ behaved similarly to the Models A, B, and C except that the compressive stresses were increased near the horizontal and vertical legs of the angles of compression top chord of the joists. From the experimental work it can be observed that the lateral deflections increased the compressive stresses near the compression chord flange (horizontal legs of top chord), vertical legs of the top chord, and the diagonal interior web members at the mid span of the HOWSJ, and this failure occurred before reached to a maximum load. Final failure was accompanied by high local buckling at the compression flange-web connection, Plate (2). And this mode of failure called flange distortional buckling.

Regarding Model B specimens it can be observed from Figures (9) and (10), that its behavior was between the behavior of Model A specimens and the behavior of Model C specimens. The experimental test showed that the lateral deflections increased the compressive stresses near the vertical legs of the top chord, the diagonal interior web members at the mid span of the HOWSJ specimens. Plate (3) shown the modes of failures for Model B specimens. And this mode of failure called lateral distortional buckling, which is possible occurs for beams with slender flexible webs and rigid flanges.

Table (3):

The average values of measured deformations for HOWSJ specimens.

Models	Ultimate Load P_u (kN)	Max. Lateral Deflection ($u_{max.}$) (mm)	Max. Rotation (ϕ_{max}) (degrees)
Model A	100.99	3.240	0.685
Model B	93.53	3.913	0.791
Model C	86.31	12.115	2.463

2.4The Effect of Cross Section Shapes of Models on the Failure Modes

Figures (9) and (10) illustrated that the lateral bending stiffness of Model A specimens are close to each other and are also close to the lateral bending stiffness of the Model B specimens, but together they have a much greater lateral bending rigidity than the Model C specimens. The reason of this large differences it was caused by the large lateral deformations occurred during the test. The reason of generated of these large deformations was may be due to the fact that the method used in the manufactured of Model A specimens ensured that the distribution of

the section materials was close to the shear center location of the section, especially the interior web members which were responsible of transfer the shear force between the top and bottom chords of the HOWSJ specimens, thus the interior web in these models were more stiffer against local buckling at the joist mid span.

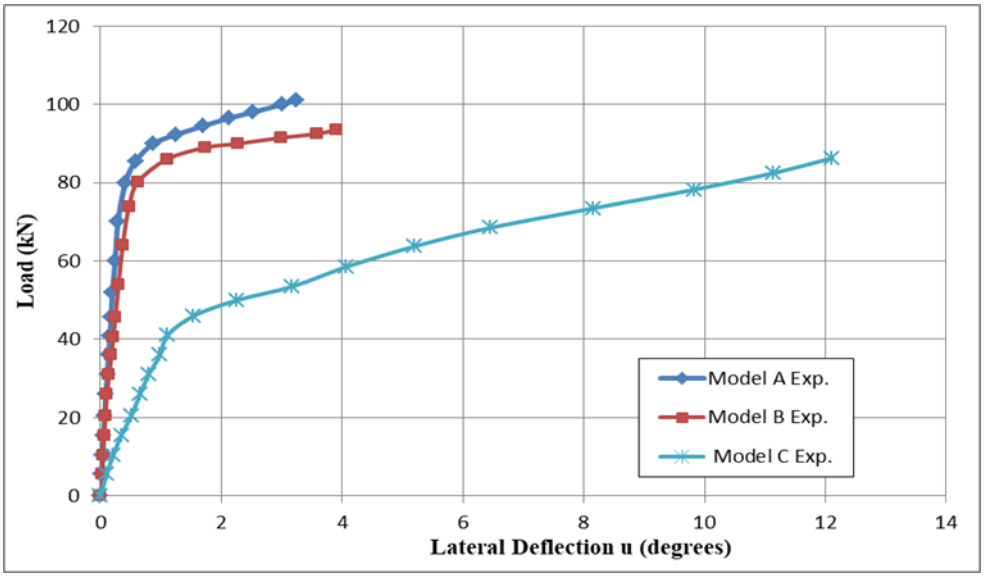

Figure 9.

Comparison of Load- Lateral Deflection Curves for all Models.

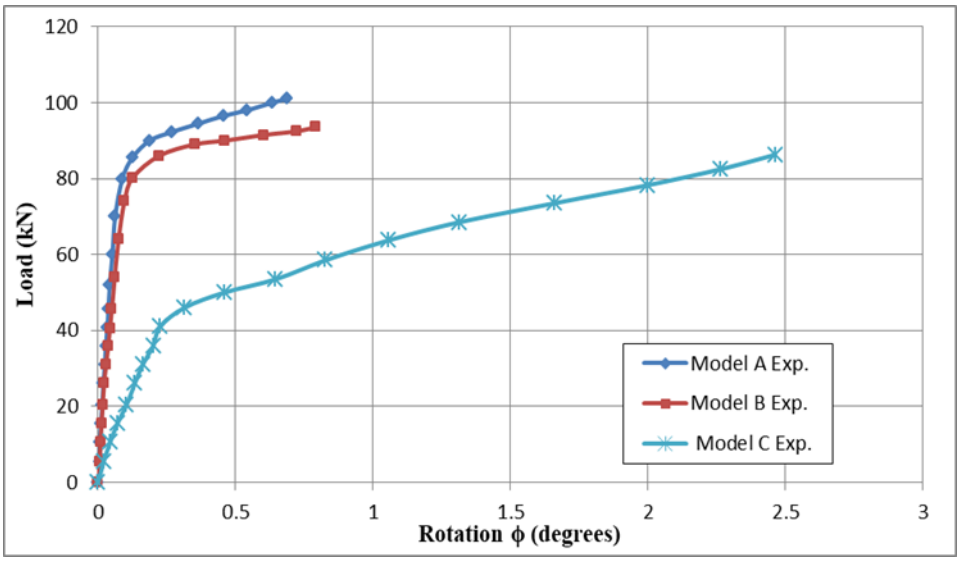

Figure 10.

Comparison of Load- Rotation Curves between HOWSJ Models

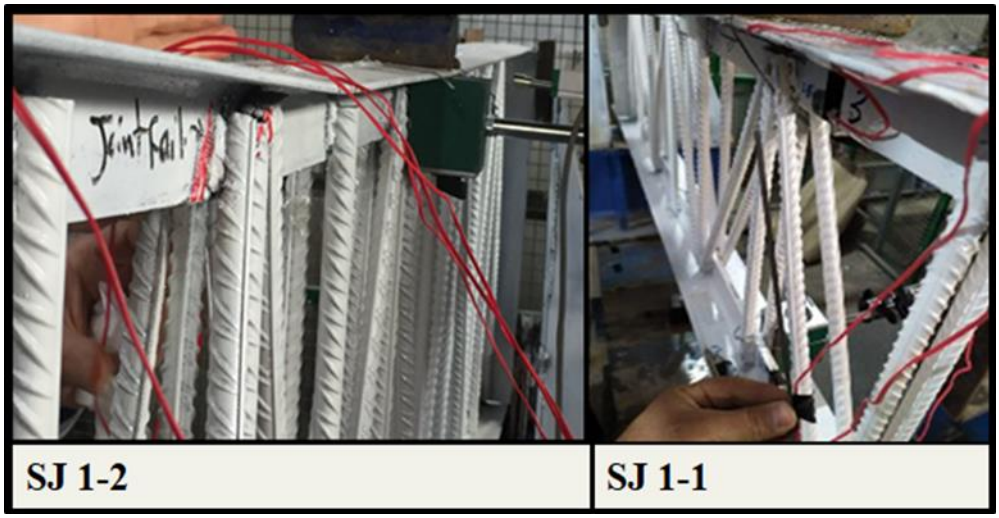

Plate (1): Failure Modes of model A Specimens.

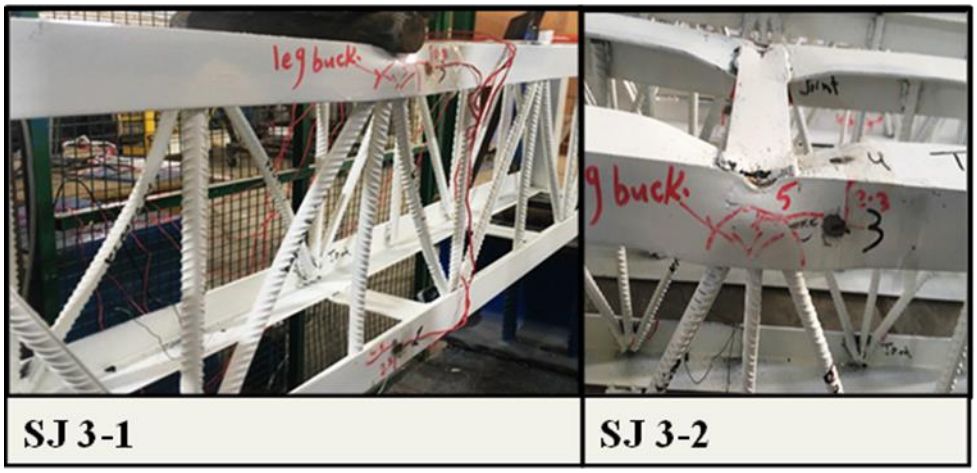

Plate (2): Failure Modes of model B Specimens.

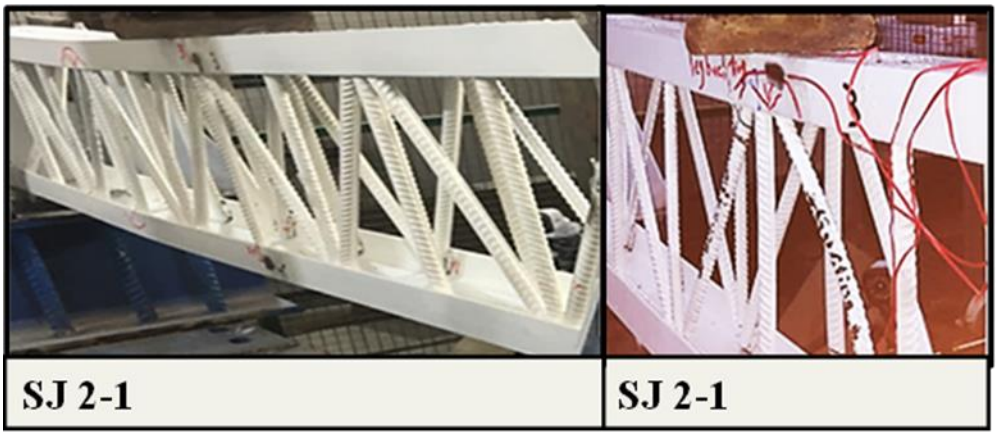

Plate (3): Failure Modes of model C Specimens.

For Model C specimens which were prefabricated with b_f of (200 mm), it can be noticed that the locations of the interior web members were far from the location of the shear center of the HOWSJ, so a torsional moment was produced because the shear forces transferred by these inner webs were become far from the shear center location. And the high local buckling occurred at the top flanges because top chord of the HOWS joist was connected together by welding a steel plate at a specified distance which made most of the horizontal legs of angles of the top chord were unrestrained against the local buckling deformations. Regarding Model B specimens' cross section which were prefabricated as their interior webs is closer to the shear center location than Model C specimens, so the local buckling of their interior webs buckled less than the interior webs used in Model C specimens. And there was no local buckling occurred in the top compression flanges because they undergo to behave as a restrained member, since the top chord flanges was manufactured by welding the horizontal legs of angle face to face at a specified distance.

2.5The Effect of the Lateral Rigidity on the Behavior of HOWSJ Models

The experimental results shown in Figures (9) and (10) suggest that the strengths of model A are methodically higher than the strengths of models B and C, which made that the comparison between the different HOWSJ models an fair, because each model had a different cross section details.

As for the models B and C which their lateral deformations were supposed to be less than the other models, because they had a greater theoretical lateral stiffness than the model A which were calculated for each cross section of the models as a built-up section as explained earlier in Table (1). This was also directly contradicted by the experimental results shown in Figures (9). (10)

As a result, in this study, a theoretical method was proposed to find an equation that allows estimating the lateral rigidity value for each model based on the details of these models' cross-sections as well as the slope of the load-lateral deflection curve (P/u) or in terms of the slope of the load-angle of twist curve $(P/\sqrt{\phi})$ which was obtained from the experimental test program to know the real behavior of each model according to the strength of its cross-section and the maximum load reached by each model. And this theoretical derived equation was shown below.

$$EI_y = \left(\frac{P}{u}\right)\frac{L^3 a}{4\pi^2} = k_1\left(\frac{P}{u}\right) \tag{2}$$

$$EI_y = \left(\frac{P}{\sqrt{\phi}}\right)\frac{\sqrt{\frac{24\,\pi^2 EI_y}{(\pi^2+6)\,P_{cr}\,L^2}}\,.\,L^3}{4\pi^2 h} = \left(\frac{P}{\sqrt{\phi}}\right)\frac{a\,.\,L^3}{4\pi^2 h} = k_2\left(\frac{P}{\sqrt{\phi}}\right) \tag{3}$$

Where: $k_1 = \frac{a\,.\,L^3}{4\pi^2}$ and $k_2 = \frac{a\,.\,L^3}{4\pi^2.h}$

The constant a can be calculated as:

$$a = \sqrt{\frac{24\,\pi^2\phi_{cr}EI_y}{(\pi^2+6)\,P_{cr}\,L^2}} = \sqrt{\phi_{cr}}\sqrt{\frac{24\,\pi^2 EI_y}{(\pi^2+6)\,P_{cr}\,L^2}} \tag{4}$$

The following equation for the static critical lateral-torsional buckling load was obtained for a simply supported HOWS joist with the effects of the warping shear stresses.

$$P_{cr} = \frac{\pi^2 EI_y h}{L^3}\left[\sqrt{\left(\frac{144}{(\pi^2+6)^2}\right)+\frac{12}{(\pi^2+6)}\left(\frac{GJ.L^2}{EC_w}+\pi^2\right)}-\left(\frac{12}{(\pi^2+6)}\right)\right] \quad (5)$$

C_w: warping torsional constant for the HOWSJ.

G : Shear modulus of elasticity

J : Saint-Venant torsional constant for HOWSJ.

E : Young's modulus of elasticity for angles.

υ = Poisson's ratio which was used =0.3 in this study.

4. THEORETICAL RESULTS OF THE LATERAL RIGIDITY

The lateral bending stiffness of the HOWS joists was calculated using Equation (3). The slope of the load- square root of the rotation curve was taken within the displacement range from (0.1 - 0.25) degrees, this range was chosen in order to avoid initial loading effects due to the attachment of the test specimen with the testing machine. The mean of two specimens for each model was be taken to find the value of lateral rigidity for each model, the results are shown in Table (4).

Table (4):

theoretical Estimation of the lateral rigidity for all models' specimens.

Model No.	**Slope ($\frac{P}{\sqrt{\phi}}$)**	P_{cr}	EI_y **(N.mm^2)**
Model A	335477	$1.271 \times 10^{-6} EI_y$	2.696×10^{11}
Model B	258689	$1.271 \times 10^{-6} EI_y$	2.078×10^{11}
Model C	131336	$1.236 \times 10^{-6} EI_y$	1.071×10^{11}

When comparing the results shown in Table (4) above, it can be noticed that the lateral rigidity of Model A increased by (60.3%) when compared with Model C and by (23 %) when compared it with Model B, the reason for the increased in lateral stiffness for this model may be due to the shape of the cross section used in its manufacture and in which the interior webs were close to the location of the shear centre, which reduced the occurrence of the torsional moment, unlike what happened with the Model B and C, where the interior webs were placed at a distance from the shear centre location, which led to the occurrence of the torsional moment, which caused buckling in the top flange , vertical leg of top chord, and in interior web . but in the other hand, it was found that the Model B had a greater lateral rigidity by (48.5%), Which made it more stable against the flange distortional buckling than the Model C, the first reason of this increasing was the width of the model was (100mm) which it was less than the width of Model C specimens , so the web in this model was closer to the location of the shear centre than the Model C, which was (200 mm), and the second it was because upper flange was welded together face to face without leaving a distance between them, which reduce the occurrence of local buckling in the top chord flanges.

Also, the strength capacity of the joist of Model C specimens was less than Model A and Model B specimens, because of these HOWSJS had weak slenderness about the y-axis; therefore, the elastic buckling occurred at the top flange when the web just had been buckled, and the compressive stress was increased on the top part of the section (compressive zone). Because of the interior webs of the joist failed to support the top flange when the compressive stress has been eliminated, then the tensile stress prevents the movement in a diagonal direction.

5. DISCUSSION OF ROTATION AND LATERAL DEFLECTION DEFORMATIONS RESULTS

After obtaining the lateral rigidity for each model, it was possible to make a normalized comparison of the different models used in this research, depending on the lateral stiffness and the ultimate load capacity for the mean value of two specimens for the same model, as shown in the Figures (11) and (12). These curves of the normalized lateral deflection ($u_{Nor.}$), and normalized rotation deformations ($\phi_{Nor.}$) showed the real behavior of all models during the test. where Equations (6) and (7) was written as shown below depending on Equations (2) and (3), respectively.

$$u_{Nor.} = \frac{u.EI_y}{k_1.P_u} \quad (6)$$

$$\phi_{Nor.} = \left(\frac{\sqrt{\phi}.EI_y}{k_2.P_u}\right)^2 \quad (7)$$

where P_u: the ultimate load capacity for each model.

The specimens of models A, B, and C, which had different cross section shapes, had more lateral deformations than Model B specimens about (19.2%) for rotation and about (21.9%) for lateral deflection, as shown in these Figures and Table (5). Furthermore, Model A specimens outperformed Model C specimens for rotation (25.1%) and lateral deflection (30.7%).

As a result, the deformations of Model B specimens exceeded those of Model C specimens by approximately (7.3%) for rotation and (11.2%) for lateral deflection. Although the top chord flanges of the Model C specimens' model experienced local buckling before reaching their ultimate capacity, this buckling occurred because their top flanges were welded face to face with a gap between them, causing the horizontal leg of the angles of the top chord to behave as an unrestrained member against distortional buckling.

According to the previous comparisons, the Model C cross section, in which the top and bottom chords of the HOWSJ were face to face with gab and welded together at equal spacing, was more stable against lateral deformations than the Model A and Model B specimens.

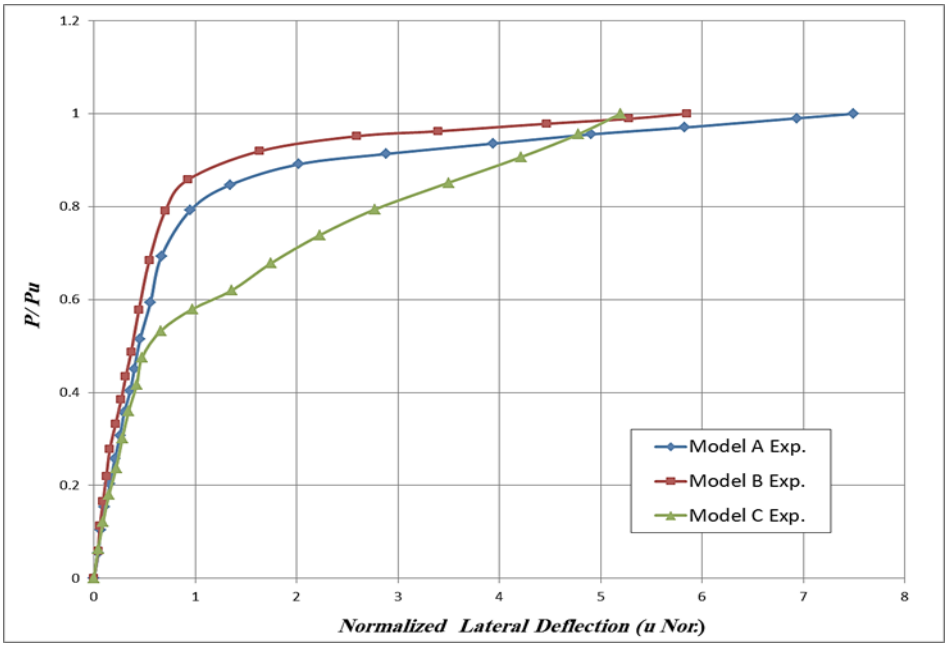

Figure (11):

Normalize Load- Lateral Deflection Curves for all Models.

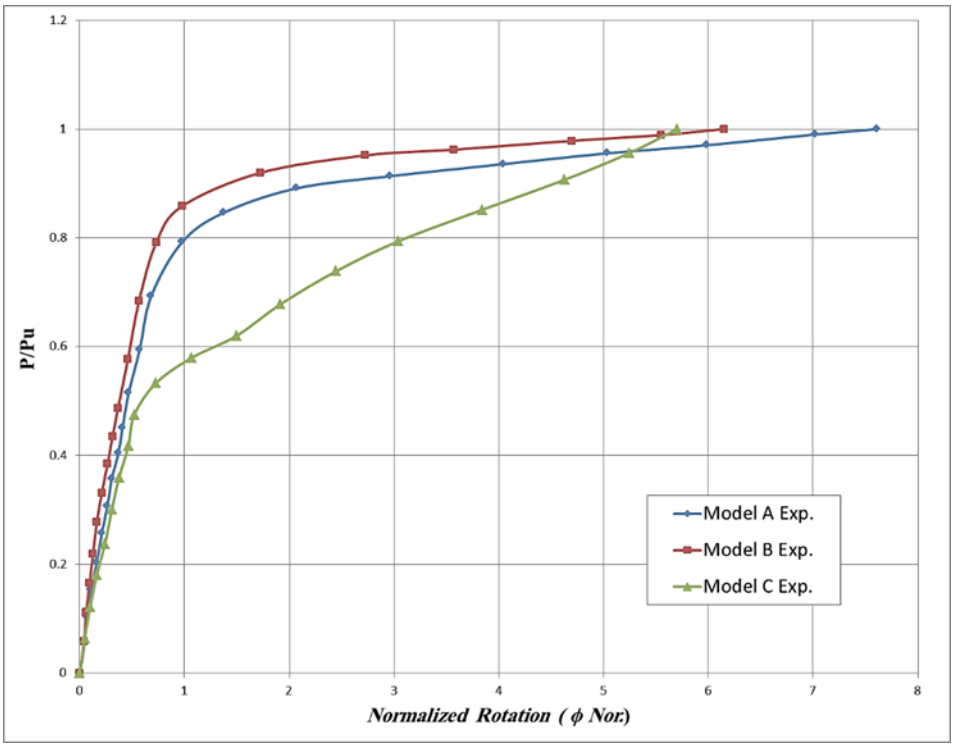

Figure (12):

Normalize Load-Rotation Curves for all models.

Table (5-4):
Normalized Lateral deflection and Rotation Deformations for all models.

Model No.	Normalized Lateral Deflection	Normalized Rotation
Model A	7.497	7.609
Model B	5.849	6.147
Model C	5.197	5.702

CONCLUSIONS

From this study the following conclusions were drawn

1- Based on the experimental results, the HOWSJ models with back-to-back welded angles cross sections had small lateral deflections and rotations while the joist was still elastic, but these increased as the load increased towards the elastic lateral buckling load and accelerated after yielding began, reaching relatively high values as the failure load was approached. Also, the ultimate failure mechanism was compression top flange buckling (horizontal leg of the top chord angles). In addition, a very small local buckling occurred in the mid span interior web member, and all HOWSJ specimens for these three models experienced slightly vertical lateral buckling during the loading phase until they reached their ultimate capacity. While there was no

buckling observed on the vertical leg of the top chord angles. This mode of failure is known as flexural lateral torsional buckling.

2- Compressive stresses were increased near the horizontal legs of the angles of compression top chord of the joists in the HOWS joists model with face to face with gap cross section. According to the experimental results, these lateral deflections increased the compressive stresses near the compression flange, vertical legs of the top chord, and interior inner web at the mid span of the HOWSJ, and this failure occurred before the maximum load was reached. At the compression flange-web connection, the final failure was accompanied by significant local buckling. This type of failure is known as flange distortional buckling.

3- In the case of HOWS joists with face-to-face without gap cross sections, the behavior was intermediate between the two previous models. Furthermore, lateral deflections increased compressive stresses near the vertical legs of the top chord and the interior inner webs in the mid span of the HOWSJ specimens. This type of failure is known as lateral distortional buckling. This is possible for beams with thin flexible webs and stiff flanges.

4- In this study, a theoretical method was proposed to find an equation that allows estimating the lateral stiffness rigidity value for each model based on the details of the cross-sections of these models as well as the slope of the lateral deformation curves obtained from the experimental test program. Using this equation, it can be observed that the lateral rigidity of Model with back-to-back cross section increased by (60.3%) when compared to Model with face-to-face cross section.

5- The specimens with the shape of the top and bottom chords of the HOWSJ was face to face with gap were more stable against lateral deformations than the other two cross sections, where they had a rotation and lateral deflection less than specimens with back-to-back welded angles by approximately (25.1%) and (30.7%), respectively. Furthermore, they had less rotation and lateral deflection than specimens with cross sections of face to face without gap welded angles by about (7.3%) and (11.2%), respectively.

6- Flexural lateral torsional buckling occurred in the HOWSJ specimens with back-to-back welded angle chords, with all HOWSJ specimens having slightly lateral buckling during the loading phase until they reached their ultimate capacity. There was no evidence of local buckling on the vertical leg of the top chord angles. In addition, a very minor local buckling in the mid span interior web member occurred.

7- The experimental test revealed that lateral deflections increased compressive stresses near the vertical legs of the top chord and the interior inner webs in the mid span of the HOWSJ specimens with chords that were face to face without gap welded angles. This type of failure is known as lateral distortional buckling.

8- Finally, the experimental test of specimens with face-to-face chords with gap welded angles revealed that lateral deflections increased compressive stresses near the compression chord flange, vertical legs of the top chord, and interior web members at the mid span of the HOWSJ, and this failure occurred before the maximum load was reached. At the compression flange-web connection, the final failure was accompanied by significant local buckling. This type of failure is known as flange distortional buckling.

REFERENCES

[1] Timoshenko S P and Gere J M 1961 *Theory of Elastic Stability* 2nd ed, New York: Mc Graw-Hill.

[2] Bradford M A and Wee A 1994 *Analysis of Buckling Tests on Beams on Seat Supports J.Constructional Steel Research*.**28**(3) pp 227 – 242.

[3] Zirakian T and Showkati H 2007 *Experiments on distortional buckling of I-beams* J. *Structural Engineering*. 133(7) pp 1009 –17.

[4] American Institute of Steel Construction AISC March 9. *Specification for structural steel buildings* (AISC 360 – 05) 2005.Chicago (IL).

[5] Standards Association of Australia (AS 4100) 1990 *Steel Structures*. Sydney, Australia.

[6] Winter G, Lansing W, and McCalley R B. Jr. (1949). ‘‘Performance of laterally loaded channel beams.’’ Proc., Symp. on Engrg. Struct., Colston Research Society, Butterworth Scientific, London, 49–60.

[7] Put BM, Pi YL, Trahair NS. Lateral buckling tests on cold-formed channel beams. Research Report No. R767, Centre for Advanced Structural Engineering, Department of Civil Engineering, The University of Sydney, Australia; 1998.

[8] Pi YL, Put BM, Trahair NS. Lateral buckling strengths of cold-formed channel section beams. Journal of Structural Engineering 1998;124(10):1182–91.

[9] Zhao XL, Hancock G, Trahair N. Lateral-buckling tests of cold-formed RHS beams. Journal of Structural Engineering 1995;121(11):1565–73.

[10] Chu XT, Kettle R, Li LY. Lateral torsional buckling analysis of partial-laterally restrained thin-walled channel-section beams. Journal of Constructional Steel Research 2004;60(8):1159–75.

[11] Nirosha D K, Mahen. Behaviour and design of cold-formed steel beams subject to lateral–torsional buckling. Journal of Thin-Walled Structures, 2012; (51): 25-38.

[12] ASTM A370 − 15, “Standard Test Methods and Definitions for Mechanical Testing of Steel Products”, West Conshohocken, PA 19428-2959, United States, United States: ASTM International, 2015.

[13] AWS A5.1/A5.1M:2004, Specification for Carbon Steel Electrodes for Shielded Metal Arc Welding. American Welding Society.